Ionics (2020) 26:4201–4212
https://doi.org/10.1007/s11581-020-03564-y

ORIGINAL PAPER

An effective strategy to enhance the photocatalytic performance by forming NiS/rGO heterojunction nanocomposites

Priyadharsan Arumugam[1] · Prabhu Sengodan[2] · Navaneethan Duraisamy[3] · Ramesh Rajendran[2,4] · Vasanthakumar Vasudevan[5]

Received: 26 September 2019 / Revised: 2 March 2020 / Accepted: 5 April 2020 / Published online: 18 April 2020

Abstract

Exploiting novel, low cost, and efficient photocatalysts for removal of pollutant waste water was significant to resolve the energy crisis and environment remediation. Here, we report the synthesis of nickel sulphide (NiS)/reduced graphene oxide (rGO)-based heterojunction photocatalyst using one step hydrothermal method. The intimate contact between NiS and rGO was suggested to quicken the transfer of photogenerated electrons from NiS to rGO, reducing the recombination of charge transporters and hence increasing the photocatalytic activities. The physico-chemical properties of the NiS/rGO heterojunction photocatalysts were scientifically studied with different characterization methods. The most efficient photocatalytic performances under solar light irradiation have been carefully assessed, and the NiS/rGO heterojunction nanocomposites exhibit photocatalytic degradation on methylene blue (MB). The removal percentage for MB can reach maximum at ~ 87% in ~ 100 min under solar light treatment. Moreover, the NiS/rGO heterojunction nanocomposite revealed highly stable for removing MB even after four successive experiments. Therefore, the experimental results demonstrated that the prepared NiS/rGO nanocomposites showed significant photocatalytic performance, thus supporting probable active heterojunction nanocomposite for energy conversion as well as in environmental remediation.

Keywords NiS/rGO nanocomposites · Photocatalyst · Heterojunction · Dye removal

Introduction

The environmental contamination produced by organic pollutants with industrialization and population growth has become a serious concern all over the world. The biggest concern is the energy lessening and environmental problems, methods using limitless solar light to catalyze particular solutions like production of hydrogen from water splitting, reduction of CO_2 into hydrocarbon fuels, in addition to decomposition of environmental pollutant fascinate several attentions [1–4]. Used for these applications, the principal is very active photocatalysts which retain comparable reaction mechanisms containing materialization of photo-generated transporters and corresponding redox reactions [5–8]. Photocatalytic methodology has turn into an ideal green technique as it can remove contaminant organic impurities in wastewater to create non-hazardous materials, for example, CO_2, H_2O and the rest with no ancillary pollution, minor reaction circumstances, and low energy consumption [9–11]. Specifically, metal sulphide-based semiconductors have fascinated varied consideration in the field of environmental decontamination and numerous attainments have been reached [12–14].

However, conservative identical photocatalyst has intrinsic disadvantages like the fast recombination of photo-induced electron-hole (e^-/h^+) pairs and the light absorption only at UV region ($\lambda < 400$ nm) [15]. Emerging heterogeneous photocatalyst exists an efficient way to widen the range of light absorption wavelengths and support the separation of

✉ Navaneethan Duraisamy
naveennanoenergy@gmail.com

[1] Department of Physics, E.R.K Arts and Science College, Erumiyampatti, Tamil Nadu, India

[2] Department of Physics, Periyar University, Salem, Tamil Nadu, India

[3] Department of Chemistry, J.K.K.Nataraja College of Arts and Science, Komarapalayam, Namakkal, Tamil Nadu, India

[4] Center for New and Renewable Energy, Department of Physics, Periyar University, Salem, Tamil Nadu, India

[5] Department of Chemistry, Periyar University, Salem, Tamil Nadu, India

the charge carrier [16–18]. Thus, the heterogeneous photocatalyst consistently displays more engaging than its identical complement. In recent times, synthesis of metal sulphide (ZnS, CdS, SnS_2, and MoS_2) based photocatalysts has been widely studied because of their widespread applications in multidisciplinary areas [19–24]. A combination of two dissimilar semiconductors inclined to prepare a nanocomposite photocatalyst is an enormously important procedure for environmental applications. Furthermore, recent investigators have presented an emergent attention favoring the production of reduced graphene oxide (rGO) based binary heterojunction nanocomposite, which can solely carry a synergistic outcome [25, 26].

The combination of rGO with a metal sulphide photocatalyst can improve photocatalytic performance due to the outstanding benefits; it offers and fulfill practical necessities [27–29]. With an existing combination of distinct graphene and semiconductor nanoparticles, the graphene seeming interacts with plentiful inorganic materials to enhance the photocatalytic activity of organic dyes [30–32]. Trending research focuses have been contributed to improving the photocatalytic performance of ZnS/rGO, SnS_2-$BiFeO_3$/reduced graphene oxide, MoS_2/RGO, and CdS/RGO nanocomposites [33–36]. An aggregation of metal sulphide with rGO is able to increase the photocatalytic performance. It is appealed that enhanced photocatalysis by rGO is owing to the incident that rGO delivers way for charge carriers.

Following the above facts, we have synthesized NiS/rGO heterojunction nanocomposites via a simple hydrothermal method. The prepared photocatalyst is assessed using different microscopic and spectroscopic methods to discover its physical and chemical properties. Moreover, the composite sample exhibits twice the degradation percentage of the photocatalytic activity in solar light irradiation. The systematic mechanism of photocatalytic dye removal is suggested for the degradation of MB, where explained in the existing research. We hope that this existing work can deliver as an origin to promote proposal of NiS/rGO heterojunction nanocomposite catalyst for waste water decontamination and other environmental applications.

Materials and methods

Materials and reagents

Graphite powders and sodium hydroxide (NaOH) were purchased from Sigma-Aldrich. Nickel (II) chloride hexahydrate ($NiCl_2.6H_2O$) and sodium Sulfide hydrate ($Na_2S{\cdot}9H_2O$) were purchased from High media. Potassium permanganate ($KMnO_4$), hydrochloric acid (HCl), sulfuric acid (H_2SO_4), hydrogen peroxide (H_2O_2), and methylene blue dye were purchased from Merck Chemicals, India, and used as purchased without any extra purification process.

Preparation of NiS/rGO heterojunction nanocomposite

Graphene oxide was synthesized through a modified Hummer's method [20]. NiS/rGO heterojunction nanocomposites were prepared using one-step hydrothermal method. In brief, 0.30 g of rGO containing 30-mL deionized water was kept for ultra-sonication for 1 h. Then, aqueous solutions of $NiCl_2.6H_2O$ (0.25 M) were added to the above suspension with continuous stirring. After 30 min of stirring, the above solution was shifted to a 100-mL Teflon-lined stainless-steel autoclave and hydrothermally treated at 170 °C for 5 h. Later cooling to ambient temperature, the obtained product was separated by centrifugation and washed several times with water and ethanol. The resulting sample was collected and then kept for drying at 60 °C overnight prior to characterization.

Characterization

Powder X-ray diffraction (XRD) analyses were recorded on a Rigaku Miniflex X-ray diffractometer with monochromatic high intensity Cu Kα radiation ($\lambda = 0.15406$ nm). FT-IR spectra were recorded on a BRUCKER TENSOR 27 FTIR spectrophotometer. The morphology analysis of NiS/rGO was carried out by scanning electron microscopy (SEM, Zeiss18 Evaluation) and high-resolution transmission electron microscopy (HRTEM, JEM-2100F, JEOL) operating at 200 kV. The optical properties of the prepared samples were measured by a V-770 diffuse reflectance spectrophotometer (DRS, JASCO). The photoluminescence (PL) study was characterized by JASCO FP-6500 using an excitation wavelength of 420 nm.

Photocatalytic degradation test

Solar light irradiation was used as an essential tool to determine the catalytic performance of the prepared nanocomposite and to measure the methylene blue degradation as well. Photocatalytic experiments were carried out with a known amount (100 mg) of prepared nanophotocatalyst composites suspended in 100 mL of MB dye solution (30 mg/mL). Before starting the photocatalytic degradation experiment, the solutions were magnetically stirred for 30 min in a dark atmosphere to establish the adsorption/desorption equilibrium of the dye molecules. The suspension then constantly irradiated with solar light for 100 min. At regular time intervals, 3 ml of the suspension was taken for centrifugation to separate the photocatalyst and for further evaluation using a UV–vis absorption spectrometer. As for the recycling experiments, the residual photocatalyst powder was centrifuged and used up to four successive cycles for photocatalytic degradation performance of NiS/rGO heterojunction nanocomposite toward MB dye. For assessment, the self photodegradation of MB

(namely, photolysis) were also established under same environments in the absence of photocatalyst. The photo-removal efficiency percentage was calculated from the equation of $C_0{-}C/C_0 \times 100$, where C_0 and C were the symbolic representations for the concentration of organic pollutant before and after photocatalytic experiments, respectively.

Photoelectrochemical analysis

The transient photocurrent (i-t), Mott–Schottky plot (M-S), and electrochemical impedance spectroscopy (EIS) measurements were conducted using SP-150 (BioLogic Science Instruments, France) electrochemical workstation. The photoelectrochemical measurements were carried out using three-electrode cell configurations. In the experiment reference electrode (Ag/AgCl (3 M KCl)), platinum wire (counter electrode) and prepared samples were working electrode. The measurements were performed in 0.5-M Na_2SO_4 electrolyte solution and xenon lamp (150 W) was used as a solar simulator. Ten milligrams of prepared samples were dispersed in 1 mL of ethanol and 40-μl Nafion solution with the help of ultrasonication for 30 min. The dispersed solution was coated on the pre-cleaned fluorine-doped tin oxide (FTO) electrode with an active surface area of ~ 1 cm^2 by spin coating technique with 4000 rpm for 2 min. The Mott–Schottky study to apply the potential ranges from − 1.2 to 6 V. Moreover, the electrochemical impedance spectroscopy (EIS) recorded at the applied frequency range from 10-2 to 105 Hz with an AC amplitude of 10 mV under open circuit potential.

Results and discussion

Crystal structures

The crystal structures of NiS and NiS/rGO heterojunction nanocomposites were analyzed using XRD diffractogram, and the experimental results were displayed in Fig. 1. The diffraction peaks of NiS at 29.79°, 45.53°, and 54.22° correspond to (002), (102), and (110) directions, suggesting α-NiS (a = b = 3.439 nm, c = 5.352 nm), where the points and concentrations of the diffraction peaks were in good agreement with the standard JCPDS Card: 65-5762 [37, 38]. The peaks corresponding to contaminations were not observed, indicating that well-crystallized NiS was obtained under the synthetic conditions. The XRD pattern of NiS/rGO heterojunction nanocomposites is shown in Fig. 1. The composite of NiS-decorated rGO showed the diffraction peaks of NiS. But, the intensities of the peaks are weakened associating with pure NiS. Besides, there is no noticeable diffraction peak consigned to the rGO in composite, which can be attributed to that the systematic stack of rGO is smashed by the intercalation of NiS to weaken the diffraction intensity of rGO.

Fourier-transform infrared spectroscopy

The FTIR spectrum of nanostructured pure NiS and NiS/rGO heterojunction nanocomposite was shown in Fig. 2. The broad band around ~ 3400–3200 cm^{-1} was assigned to the stretching and bending mode of O–H and H–O–H groups of absorbed water. The peaks around ~ 607 cm^{-1} indicate the stretching mode of Ni–S. These peaks remain the same in the composite (NiS-rGO). Moreover, the characteristic peaks of C–O, C=O stretching would not be observed in composite, which confirmed the reduction of GO into rGO. Therefore, this outcome is evident of the purity and presence of functional groups in pure NiS and composite.

Morphological analysis

Figure 3a–c shows the FESEM images of pure NiS, rGO sheet, and composite of NiS-rGO samples. The surface morphology of rGO revealed the two dimensional (sheet structure) morphology (Fig. 3b). The rGO sheets were closely packed and aggregated due to the reduction of functional groups in GO. Furthermore, aggregations were significantly reduced in composite materials due to the interaction of NiS with rGO sheet as shown in Fig. 3c. However, partial magnification of FESEM, the morphology of NiS/rGO heterojunction nanocomposites was not perfectly demonstrated. Therefore, HRTEM were analyzed to advance a better consideration of the morphological and structural features. Figure 4a–e displays HRTEM of NiS/rGO heterojunction nanocomposite, respectively. NiS/rGO heterojunction revealed the anisotropic surface morphology due to the influence of hydrothermal treatment. It can be clearly seen a homogeneous dispersion of the nanomaterials in the rGO supports.

The lattices of NiS/rGO heterojunction were obviously evident in the HRTEM images. The adjacent interface of NiS on rGO nanoparticles (Fig. 4e) revealed the formation of nano heterojunction. This type of nanocomposite was more favorable for the transportation of photoexcited carriers between NiS and rGO. An average particle size in the range of 5–50 nm, the selected area electron diffraction (SAED) pattern of the heterojunction nanocomposites material was polycrystalline nature (Fig. 4f). The d spacing value of 0.22 nm corresponds to the (102) crystal plane of the NiS. Based on the above results, we can presume that the strong interfacial coupling effect between NiS and rGO will stimulate photogenerated electron-hole pair separation and relocation, and hence further improve the photocatalytic activity of NiS/rGO heterojunction nanocomposites [39].

Optical properties

The UV–visible diffuse reflectance spectra are conducted to investigate the optical absorption property of the NiS and NiS/

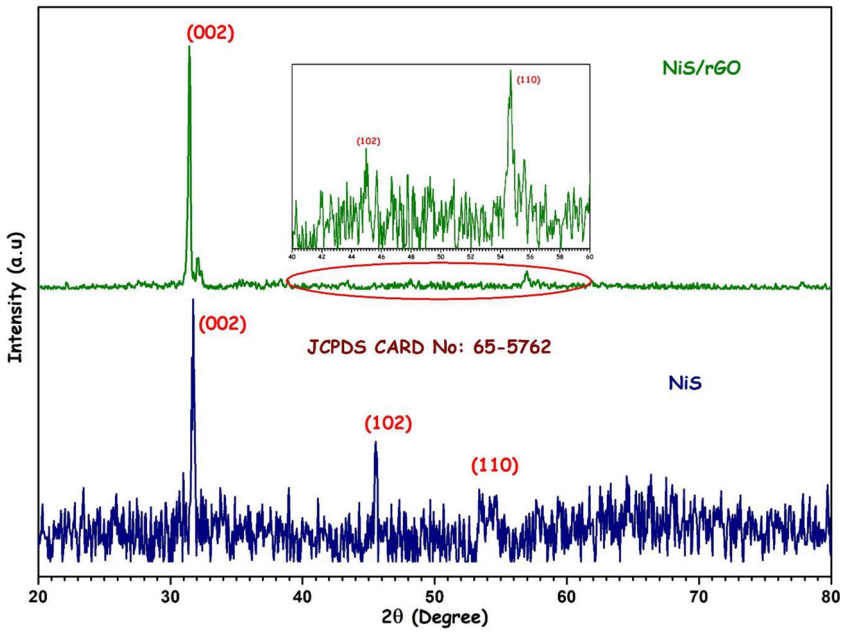

Fig. 1 XRD patterns of NiS and NiS/rGO heterojunction nanocomposites

rGO nanocomposites as shown in Fig. 5. The spectrum of the NiS/rGO heterojunction catalyst shows an enriched absorption in visible light region, from 400 to 500 nm. However, a gradual red-shift to longer wavelengths is observed for the NiS/rGO nanocomposites. The red-shift absorption is attributed to the formation of the Ni-O-C bond, which reduces the bandgap energy of the NiS/rGO nanocomposite. The NiS/rGO nanocomposites therefore show a continuously improved visible-light absorption, which is in agreement with the results. Furthermore, the outcomes showed that the NiS has low intensity absorption in UV and visible region. In the UV region, all the NiS-rGO samples have absorption with high intensities, which showed that the photocatalytic activity of NiS-rGO composites can be complete in this region.

To gain deep insight into the separation, transfer, and recombination behavior of the photogenerated charge carriers in the samples, photoluminescence emission spectra are measured as shown in Fig. 6. Compared with the pure, the NiS-rGO nanocomposites showed decrease in the PL intensity, which indicates that the recombination of the electron/hole pairs can be significantly inhibited in the composite. The experimental results indicate that the suppressed recombination of photogenerated electron–hole pairs.

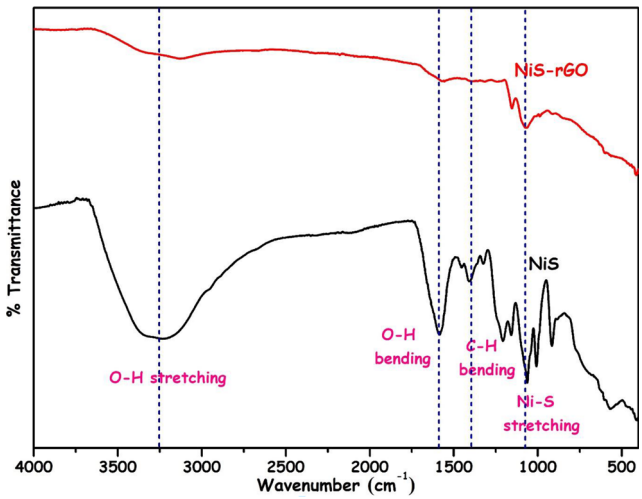

Fig. 2 FTIR spectra of NiS and NiS/rGO heterojunction nanocomposites

Photocatalytic degradation of NiS/rGO heterojunction nanocomposites

The photocatalytic activity of as-synthesized NiS/rGO heterojunction nanocomposites was assessed by observing its typical absorption band at 650 nm to calculate the degradation percentage of MB under solar light irradiation. Before light irradiation, the solutions were magnetically stirred in dark condition for 30 min to confirm the adsorption-desorption equilibrium of MB. Figure 7a, b shows the photocatalytic activity of NiS/rGO heterojunction nanocomposites. The photocatalytic degradation spectra in Fig. 7b exhibit both the adsorption and the photocatalytic degradation performance in NiS/rGO heterojunction nanocomposites, where maximized and attained the utmost adsorption ability at about 87%. In the case of pure NiS nanoparticles (Fig. 7a), the degradation of MB dye solution has reached approximately 70%, which was lower than that of NiS/rGO heterojunction.

Figure 8a, b shows the time-dependent irradiation absorption spectra of time vs. C_t/C_0 under solar light irradiation for different catalytic conditions. The results showed that the removal performance of MB could be increased in NiS/rGO heterojunction photocatalyst as associated to pure NiS. It clearly states that NiS/rGO heterojunction catalysts revealed

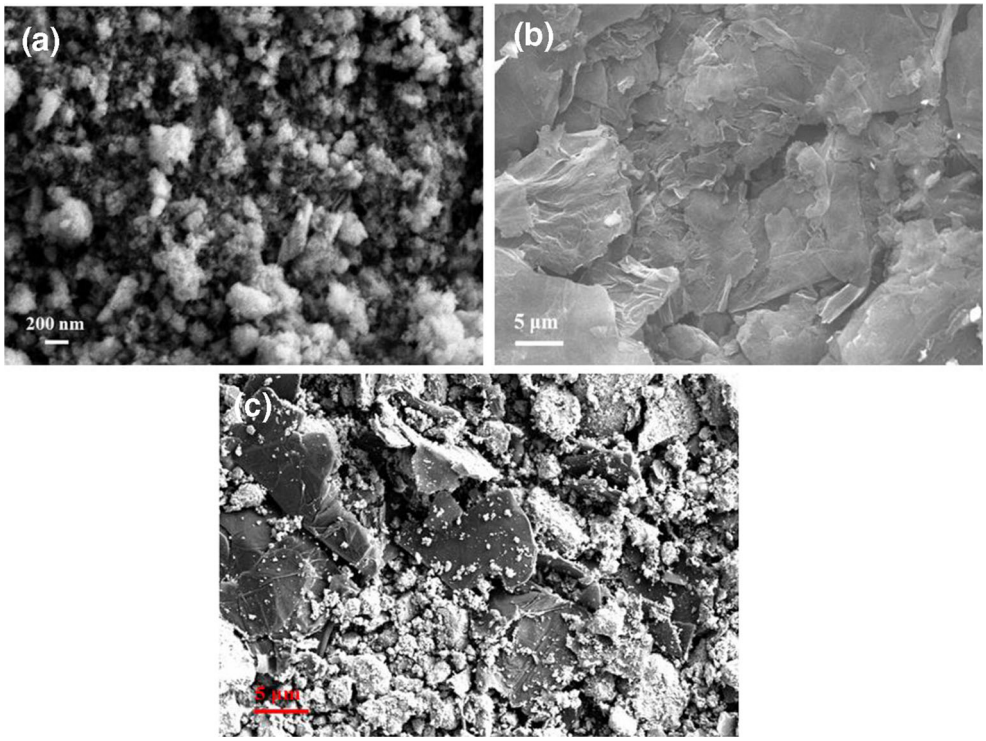

Fig. 3 FESEM analysis. **a** Pure NiS, **b** rGO, and **c** NiS-rGO heterojunction nanocomposite

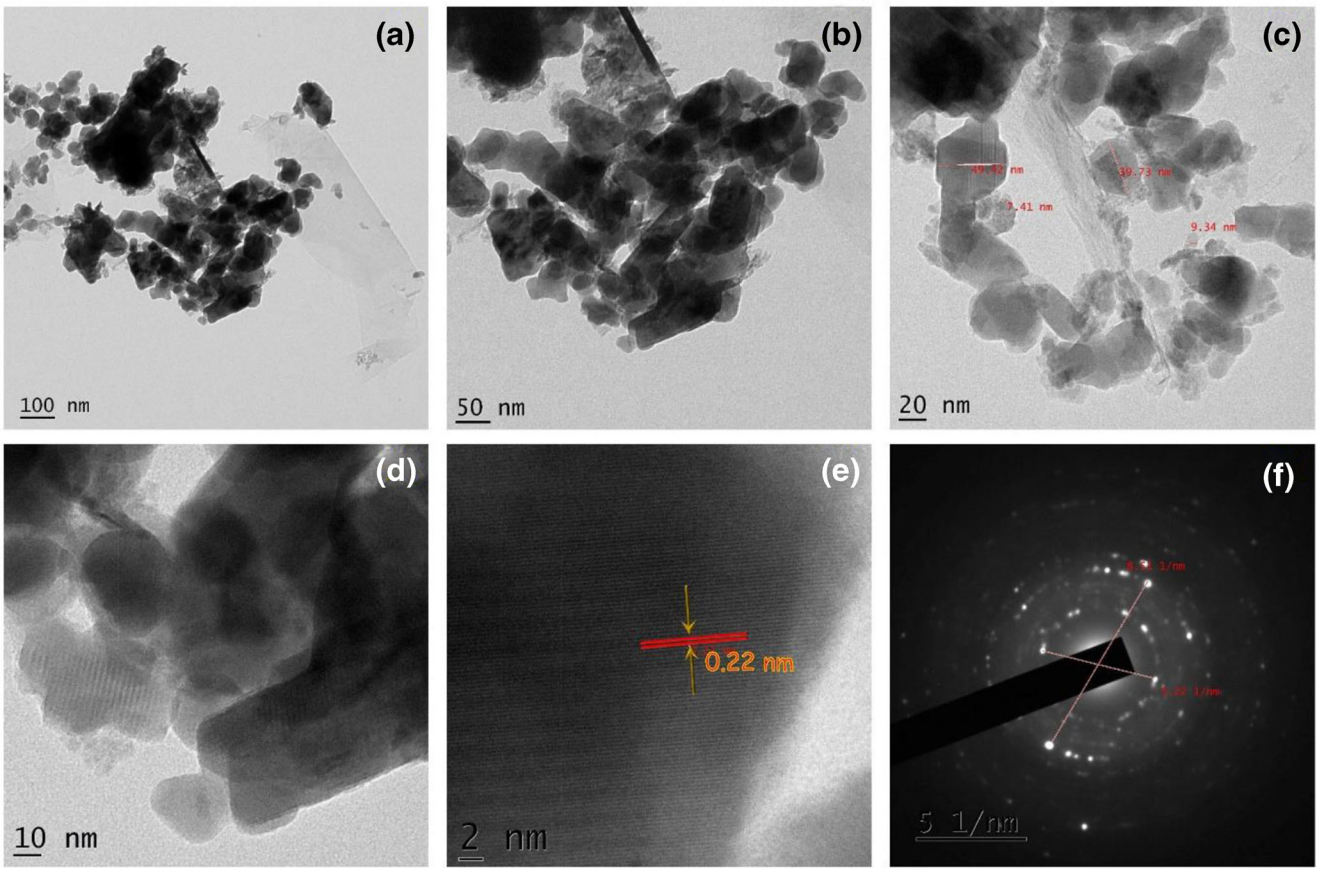

Fig. 4 **a**–**e** HR-TEM images of NiS/rGO heterojunction nanocomposites at different magnifications. **f** SAED patterns of NiS/rGO heterojunction nanocomposites

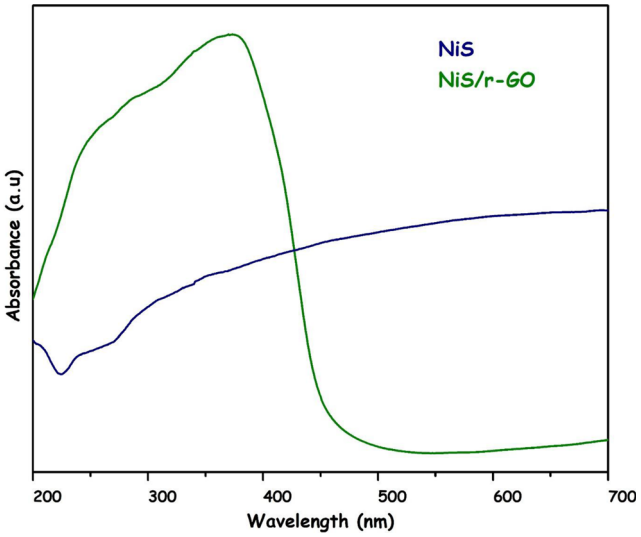

Fig. 5 UV–visible diffuse reflection spectra of NiS and NiS/rGO nanocomposite

admirable photocatalytic activity against MB oxidation. For all catalysts, over 87% of MB was degraded after 100 min, proposing substantial photolytic performance.

The photocatalytic activity kinetics of MB using prepared photocatalysts were analyzed via the pseudo first-order kinetic model to define the rate constant of photocatalytic degradation in regard to the reaction time when the first concentration of the organic pollutant was low, as the following equation: [40, 41].

$$\mathrm{In}(C_t/C_0) = -\mathrm{kt}$$

where C_0 is the initial concentration of MB, C_t is the concentration at time t, and k is the reaction rate constant. The rate constant was evaluated by the slopes of linear fit as illustrated in Fig. 8c. The values of k were 0.6015, 0.8874, 0.9794, and

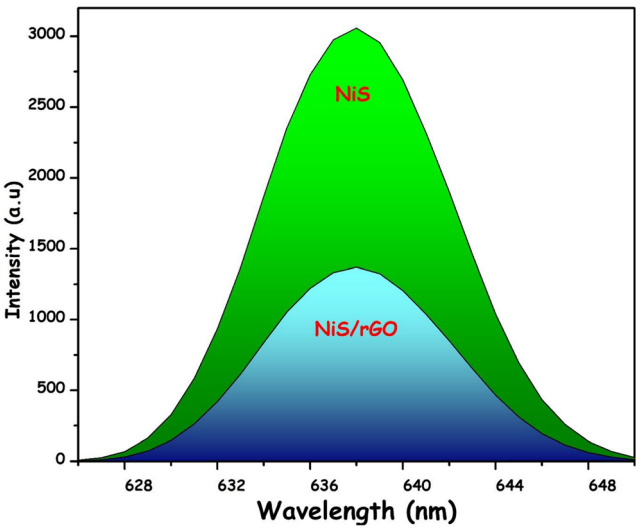

Fig. 6 Photoluminescence spectra of the NiS and NiS-rGO nanocomposite photocatalysts

$0.9989\ \mathrm{min}^{-1}$ for without, dark, NiS, and NiS/rGO heterojunction nanocomposites catalysts, respectively. Hence, the photocatalytic degradation rate of NiS/rGO heterojunction catalyst was about 3 times larger than that of NiS.

The pH is an important parameter influencing photocatalytic degradation of organic pollutants and the experiments were carried out at pH values of (3, 7, 9, and 11) in Fig. 9a. The pH was adjusted before light irradiation by concentrated solutions of sodium hydroxide (pH < 7), hydrochloric acid (pH > 7), and other parameters remain constant. Figure 9a shows that the initial pH 3 and the dye degradation efficiency were only about 44% after 100 min. Meanwhile, the degradation efficiency is up to 88% at pH 7, which is the natural pH value of di-ionized water, without pH adjustment. In addition to the photocatalytic degradation efficiency increased with the increase of pH, exhibiting maximum efficiency (94%) at pH 11, which easily adsorbs on the surface of NiS/rGO heterojunction nanocomposites, resulting in the increase of photocatalytic degradation efficiency. Moreover, OH ions are easily adsorbed on the semiconductor surface at alkaline conditions, which promotes the generation of hydroxyl free radicals and subsequently a probably higher pollutant oxidation.

Photocatalyst concentration of the range from 25 to 100 mg/L was studied and its dye concentration, reaction temperature, pH values remain constant, and the degradation efficiency is shown in Fig. 9b. The photodegradation efficiency was from 47.8 to 95% with increasing NiS/rGO nanocomposites dosage from 25 to 100 mg/L, respectively. When catalyst dosage is from 100 mg/L, the maximum photodegradation efficiency is 95% at 100 min. Many researchers have demonstrated that photodegradation efficiency of organic pollutants is strongly affected by the number of active sites and more availability photo-excited electrons and holes in the reaction solution.

Keeping the NiS/rGO nanocomposite concentration at 100 mg/L remains constant the dye solution. The effect of varying amounts of the dye was studied on degradation efficiency (10 mg/L, 15 mg/L, 20 mg/L, and 25 mg/L) as given in Fig. 9c. When increasing the concentration of MB, the rate of degradation efficiency was found to decrease. These results indicate that the number of dye molecules increase, and the amount of light passing through the dye solution to reach the catalyst surface was reduced. Thereby the formation of the reactive hydroxyl and superoxide radicals is also simultaneously reduced. Thus, there should be an optimum value maintained for the catalyst and the dye concentration, wherein maximum efficiency of degradation can be achieved.

The photocatalytic activities of NiS/r-GO photocatalyst are examined for the photodegradation of colorless phenol at room temperature (Fig. 9d). In 100 mg of NiS/rGO photocatalyst was added into 100 mL colorless phenol

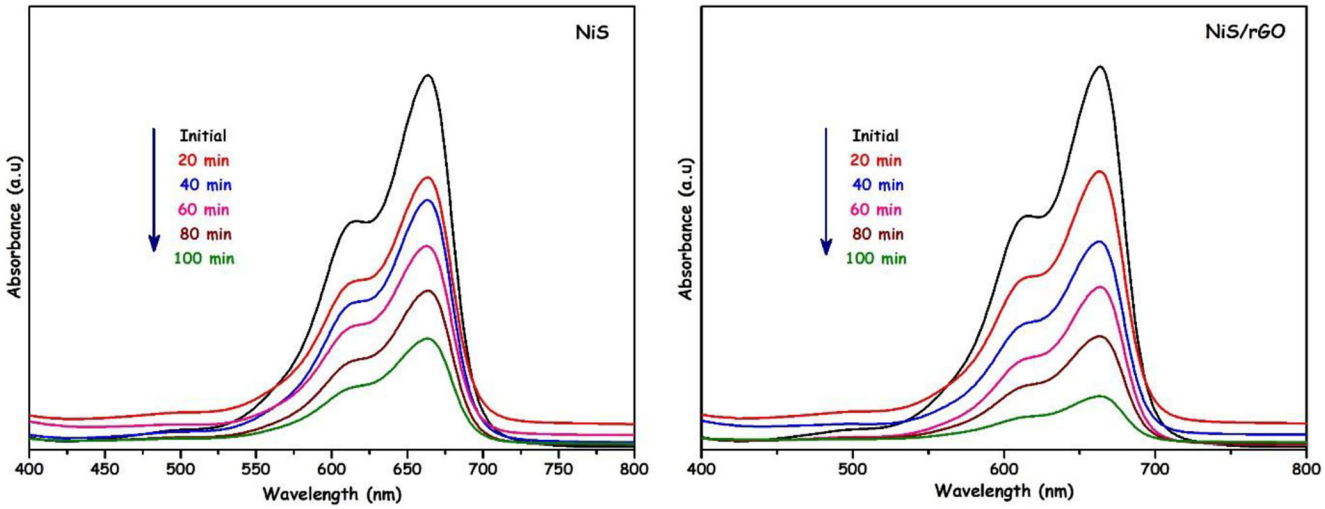

Fig. 7 Typical UV–vis spectra of MB aqueous solutions after photocatalytic degradation for various times using NiS and NiS/rGO as the photocatalyst under solar light irradiation

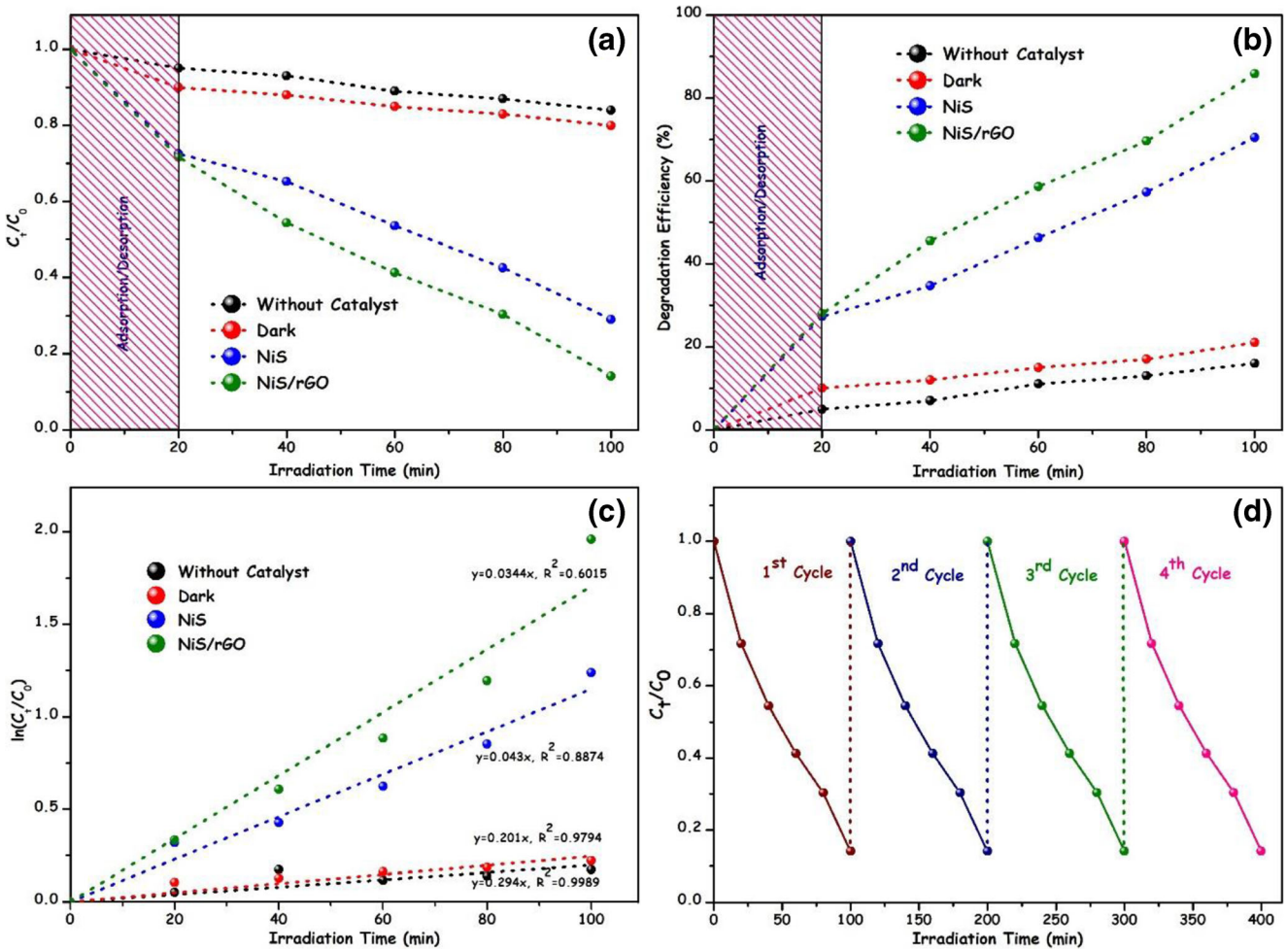

Fig. 8 Photocatalytic activity of the photocatalysts based on the photocatalytic degradation (**a**) and removal percentage (**b**) of MB under solar light irradiation, the corresponding plots of $\ln(C_t/C_0)$ vs. irradiation time of the prepared catalysts (**c**), catalysts recycling in the photodegradation of MB under solar light irradiation (**d**)

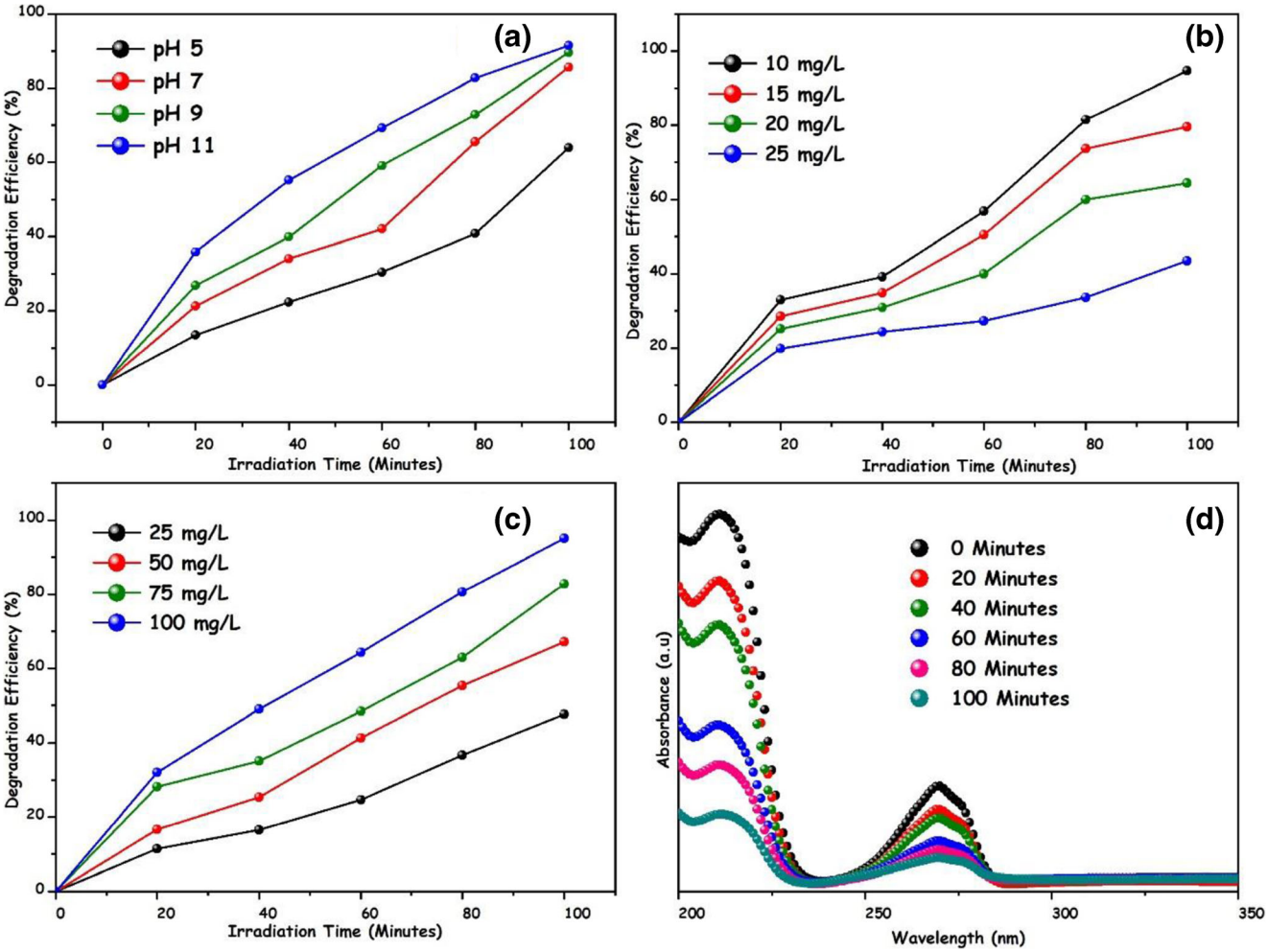

Fig. 9 Factorial effects of heterogeneous reaction on MB degradation and respective degradation efficiency spectra of high efficient degradation cycle: pH value (**a**), MB concentration (**b**), catalyst dosage (**c**), and degradation of colorless phenol (**d**)

(20 mg/L) aqua solution. Previous to the irradiation, the solution was magnetically stirred under the dark condition for 100 min to form adsorption-desorption equilibrium experiment. After that, the photocatalyst measurement was illuminated. In regular interval (20 min), 3 mL of the colorless phenol was taken and separated by centrifugation (5000 rpm) to remove the catalyst, and the colorless phenol absorption value of the supernatant was measured at 270 nm (colorless phenol) using a UV–visible spectrophotometer (JASCO V-670 double beam).

The photocatalytic evaluation of without and with NiS/rGO photocatalyst was carried out by the degradation of colorless phenol under solar light irradiation; the results are shown in Fig. 9d. As shown in Fig. 9d, the NiS/rGO photocatalyst can degrade 89.20% of colorless phenol degraded after 100 min of light irradiation. Therefore, these results conclude that the NiS/rGO photocatalyst has a prominent role to degrade the colorless phenol further improved with (~ 89%). In this result, NiS/rGO photocatalyst possessed powerful photo-oxidation ability and suggested that the photocatalysts for practical applications.

The stability and reusability of used samples were also significant aspects for their practical use. Hence, the durability reactions of NiS/rGO heterojunction nanocomposites for the removal of MB under solar light irradiation were confirmed. After every experiment, the catalyst was washed with distilled water and recycled; the outcomes can be perceived in Fig. 8d. The photocatalytic degradation efficiency shows virtually no major loss while they have been used for four successive cycles, which reveals that NiS/rGO heterojunction nanocomposites are satisfactorily constant and not disabled during the photodegradation progression. The XRD pattern of NiS/rGO(2) after the degradation of MB is measured, and shown in Fig. 10. The XRD pattern peak of the NiS/rGO(2) sample did not change much before and after the MB degradation test, suggesting that our photocatalyst is stable in structure.

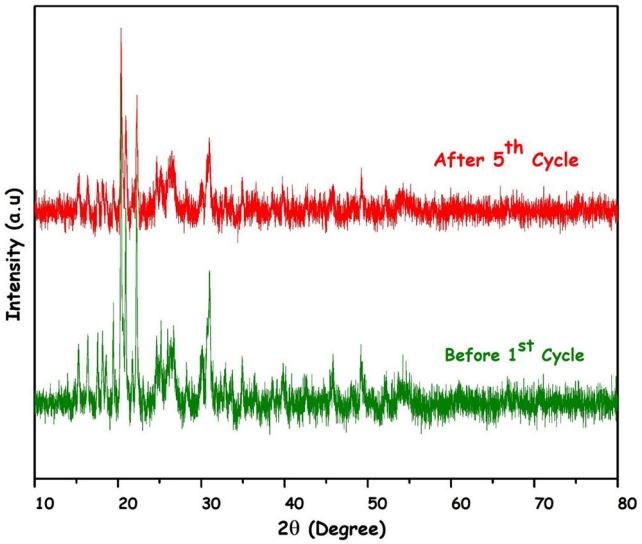

Fig. 10 XRD patterns of NiS/rGO (2) after 5 cycles recycle test toward MB degradation

Trapping and electrochemical experiments

Figure 11 shows the results of NiS/rGO heterojunction nanocomposites. Without any trapping reagent, NiS/rGO heterojunction catalyst displays the capability of contravention miserable the MB dye under solar light irradiation. In addition of the expense reagents, the removal percentage of the pollutant dye shrinkage, which means photogenerated holes, superoxide anion radicals and hydroxyl radicals were created and energetic for the duration of the photocatalytic degradation method. Specifically, an active photogenerated holes eliminate the dye-sensitization mechanism of the photodegradation because the hole was not complicated in the dye sensitization process [42].

Moreover, all four established types together with superoxide anion radical, photogenerated hole, hydroxyl radical, superoxide anion radical, and photogenerated electrons were active during the photocatalysis process. For NiS/rGO heterojunction nanocomposites, the stabilized degradation percentage with EDTA, BQ, IPA, and $AgNO_3$ was 59%, 22%, 40%, and 70%, respectively.

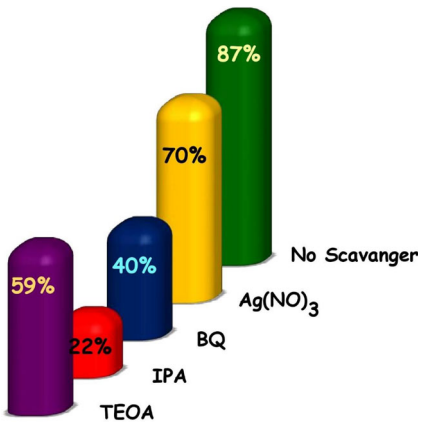

Fig. 11 Effects of a series of scavengers on the degradation efficiency of MB by NiS/rGO heterojunction photocatalyst

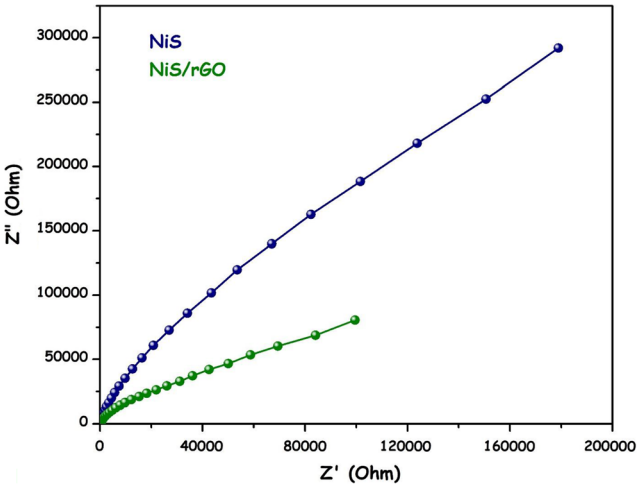

Fig. 12 Electrochemical impedance spectroscopy (EIS) plots of NiS and NiS/rGO nanocomposites

Electrochemical impedance spectroscopy (EIS) analysis is further performed to understand the fundamental electron transfer kinetics, and the corresponding Nyquist plot of EIS spectra for NiS and NiS/rGO catalysts is presented with the difference of impedance, |Z|, as a function of frequency as shown in Fig. 12. The charge carrier dynamics at the interface between the photoanode and the electrolyte could be analyzed using EIS. The diameter of the semicircle in the Nyquist plot could be an indicator of the resistance of charge transfer from photoanode to electrolyte. From Fig. 12, it is clear that rGO ornamentation shows a remarkable rise of charge transfer efficacy that results in a slighter arc than that of pure NiS. Moreover, NiS/rGO heterojunction shows the minutest arc associated to the pure, indicating that the charge transfer is considerably enhanced by both NiS and rGO.

In general, photocurrent value could provide a directory to the sample's capability to produce and transfer the

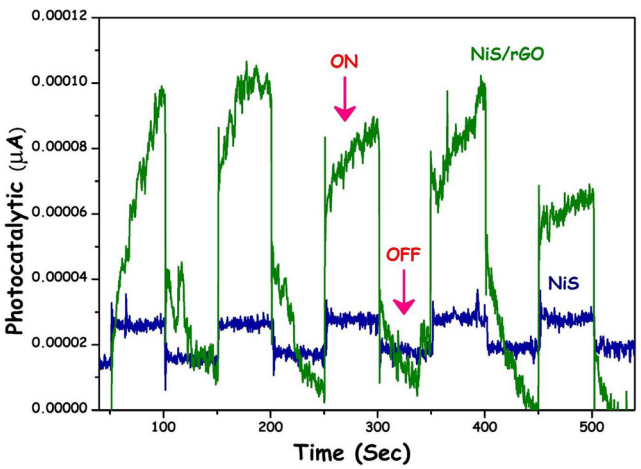

Fig. 13 Photocurrent responses of the NiS and NiS/rGO nanocomposites

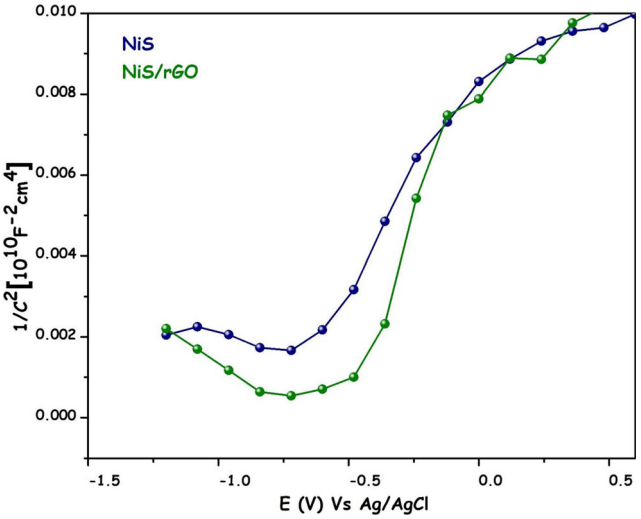

Fig. 14 Mott-Schottky curves for the NiS and NiS/rGO nanocomposites in an aqueous solution of Na_2SO_4 as supporting electrolyte

photogenerated charge carriers secondarily, which influences catalyst photocatalytic efficiency to a large degree (Dong et al. 2014). The photocurrent plots of the NiS and NiS/rGO nanocomposites under solar light irradiation are shown in Fig. 13. The photocurrent for NiS/rGO heterojunction is nearly 4.5 times as much as the NiS catalyst which showed the faster charge transfer and more efficient separation of electron-hole pairs through the NiS/rGO nanocomposites, which can significantly improve the photocatalytic performance toward MB degradation.

Figure 14 shows the hydrogenation and NiS decoration lead to the cathodic shift of the flat band potential using Mott–Schottky measurements, which proposes the enhanced photogenerated charge separation. Furthermore, the smaller Mott–Schottky plot slope of NiS/rGO compared with the NiS indicates its increased donor density. However, an observable increase of electron density is perceived for the NiS/rGO, signifying that the introduction of NiS with rGO played an imperative role in improving electron density of NiS/rGO nanocomposites. So, more electrons can participate in photocatalytic MB degradation process.

Photocatalyst mechanism

Based on the overhead investigational results and discussion, a probable mechanism for photodegradation of MB dye solution under solar light driven NiS/rGO heterojunction nanocomposite was suggested and showed in Fig. 15. In the composite, NiS and rGO sheets were active to solar light.

The higher activity of NiS/rGO heterojunction catalyst could be contributed to the photoexcited, which shows NiS/rGO nanocomposites absorbs light of the solar light and produces photo-generated charge transporters (holes and electrons). Though, to enhance the photocatalytic performance of NiS was devoted to a rGO, meanwhile rGO was an electron accepter/carrier that acts as a significant role in the separation of the carrying electron-hole pairs in the heterojunction system [43]. The excited electron in the conduction band of NiS can be suitably shifted to the rGO sheet, which slows down the recombination of the electron-hole pairs and improves the plenty and constancy of photogenerated charge in the heterojunction for the photo degradation of MB dye solution.

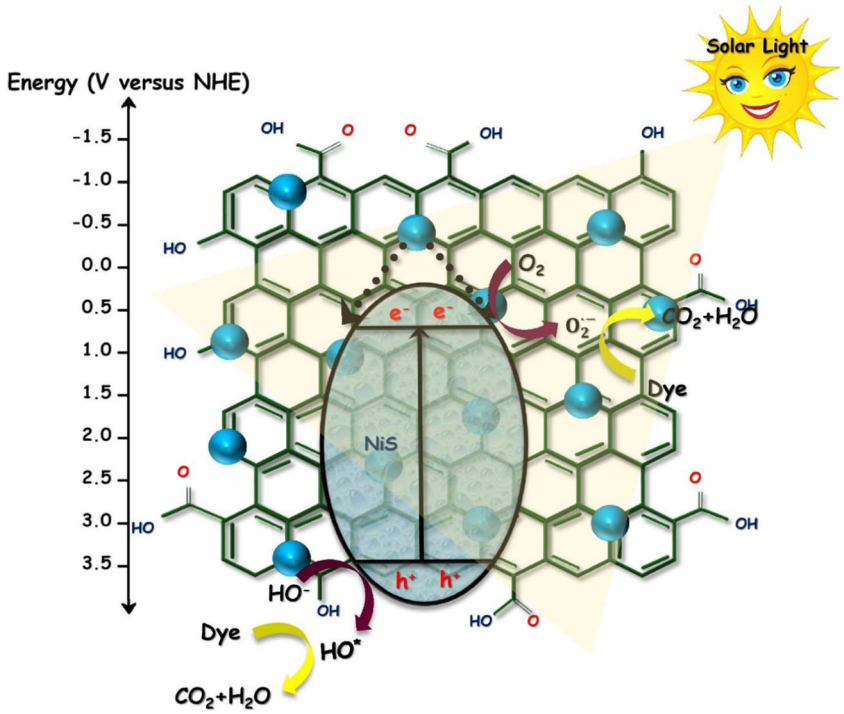

Fig. 15 Proposed mechanisms of photogenerated charge transfer and pollutants degradation in the NiS/rGO heterojunction nanocomposites under solar light irradiation

Simultaneously, the remote photogenerated charges support the creation of reactive oxidative species, i.e., $O_2^{\bullet-}$ and $OH^{\bullet}$, which were liable for degrading MB dye solution verified by Fig. 15.

Conclusion

In summary, a simple photocatalytic material was prepared using facile synthesis method. In this reaction system, the structures of NiS/rGO heterojunction nanocomposites own different boundary exposed active surface and we detected its photocatalytic degradation activity under the solar light irradiation. The FESEM and HRTEM images of the heterojunction catalyst showed that NiS has hexagonal morphology, that are uniformly dispersed on the rGO sheets, and the average particle size of the heterojunction is confirmed to be from 5 to 50 nm. The rGO-based NiS nanocomposite resulting from the heterojunction assembly extant excited charge carriers with the coupling effect of NiS and rGO, refining the recombination time. The obtained NiS/rGO heterojunction revealed the superior photocatalytic performance against MB degradation under solar light irradiation as compared with pure NiS. Moreover, NiS/rGO nanocomposite revealed better solar light photocatalytic constancy and reusability. Hence, the development of such hierarchical metal sulphide/reduced graphene oxide nanocomposites provides a more effective economical approach to harvest solar energy for decomposition of highly dangerous MB dyes from the wastewater.

Acknowledgments Dr. Navaneethan Duraisamy acknowledges the DST, New Delhi, India, for the DST Inspire Faculty award (DST/INSPIRE/04/2018/001444).

References

1. You B, Liu X, Jiang N, Sun Y (2016) A general strategy for decoupled hydrogen production from water splitting by integrating oxidative biomass valorization. J Am Chem Soc 138:13639–13646. https://doi.org/10.1021/jacs.6b07127
2. Bagheri S, Termehyousefi A, Do TO (2017) Photocatalytic pathway toward degradation of environmental pharmaceutical pollutants: structure, kinetics and mechanism approach. Catal Sci Technol 7:4548–4569. https://doi.org/10.1039/c7cy00468k
3. Roy SC, Varghese OK, Paulose M, Grimes CA (2010) Toward solar fuels: photocatalytic conversion of carbon dioxide to hydrocarbons. ACS Nano 4:1259–1278
4. Jahurul Islam M, Amaranatha Reddy D, Han NS, Choi J, Song JK, Kim TK (2016) An oxygen-vacancy rich 3D novel hierarchical MoS_2/BiOI/AgI ternary nanocomposite: enhanced photocatalytic activity through photogenerated electron shuttling in a Z-scheme manner. Phys Chem Chem Phys 18:24984–24993. https://doi.org/10.1039/c6cp02246d
5. Liu M, Sun J, Sun JDS et al (2015) Recent developments in heterogeneous photocatalytic water treatment using visible light-responsive photocatalysts: a review. RSC Adv 5:14610–14630. https://doi.org/10.1039/c4ra13734e
6. Islam MJ, Reddy DA, Choi J, Kim TK (2016) Surface oxygen vacancy assisted electron transfer and shuttling for enhanced photocatalytic activity of a Z-scheme CeO_2-AgI nanocomposite. RSC Adv 6:19341–19350. https://doi.org/10.1039/c5ra27533d
7. Lee S, Amaranatha Reddy D, Kim TK (2016) Well-wrapped reduced graphene oxide nanosheets on $Nb_3O_7(OH)$ nanostructures as good electron collectors and transporters for efficient photocatalytic degradation of rhodamine B and phenol. RSC Adv 6:37180–37188. https://doi.org/10.1039/c6ra05169c
8. Reddy DA, Choi J, Lee S, Kim TK (2016) Controlled synthesis of heterostructured Ag@AgI/ZnS microspheres with enhanced photocatalytic activity and selective separation of methylene blue from mixture dyes. J Taiwan Inst Chem Eng 66:200–209. https://doi.org/10.1016/j.jtice.2016.06.022
9. Shajahan S, Arumugam P, Rajendran R, Ponnusamy Munusamy A (2017) Optimization and detailed stability study on Pb doped ceria nanocubes for enhanced photodegradation of several anionic and cationic organic pollutants. Arab J Chem. https://doi.org/10.1016/j.arabjc.2017.11.001
10. Deng W, Zhao H, Pan F, Feng X, Jung B, Abdel-Wahab A, Batchelor B, Li Y (2017) Visible-light-driven photocatalytic degradation of organic water pollutants promoted by sulfite addition. Environ Sci Technol 51:13372–13379. https://doi.org/10.1021/acs.est.7b04206
11. Fabbri D, López-Muñoz MJ, Daniele A et al (2018) Photocatalytic abatement of emerging pollutants in pure water and wastewater effluent by TiO_2 and Ce-ZnO: degradation kinetics and assessment of transformation products. Photochem Photobiol Sci. https://doi.org/10.1039/c8pp00311d
12. Wu N (2018) Plasmonic metal-semiconductor photocatalysts and photoelectrochemical cells: a review. Nanoscale 10:2679–2696. https://doi.org/10.1039/c7nr08487k
13. Yang L, Zhou H, Fan T, Zhang D (2014) Semiconductor photocatalysts for water oxidation: current status and challenges. Phys Chem Chem Phys 16:6810–6826. https://doi.org/10.1039/c4cp00246f
14. Li J, Wu N (2015) Semiconductor-based photocatalysts and photoelectrochemical cells for solar fuel generation: a review. Catal Sci Technol 5:1360–1384. https://doi.org/10.1039/c4cy00974f
15. Priyadharsan A, Vasanthakumar V, Shanavas S et al (2019) Crumpled sheet like graphene based WO_3-Fe_2O_3 nanocomposites for enhanced charge transfer and solar photocatalysts for environmental remediation. Appl Surf Sci 470:114–128. https://doi.org/10.1016/j.apsusc.2018.11.130
16. Wei L, Yu C, Zhang Q et al (2018) TiO_2-based heterojunction photocatalysts for photocatalytic reduction of CO_2 into solar fuels. J Mater Chem A 6:22411–22436. https://doi.org/10.1039/C8TA08879A
17. Li D, Shi F, Jiang D et al (2017) $CdIn_2S_4$/g-C_3N_4 heterojunction photocatalysts: enhanced photocatalytic performance and charge transfer mechanism. RSC Adv 7:231–237. https://doi.org/10.1039/C6RA24809H
18. Adhikari SP, Hood ZD, Chen VW et al (2018) Visible-light-active g-C_3N_4/N-doped $Sr_2Nb_2O_7$ heterojunctions as photocatalysts for the hydrogen evolution reaction. Sustain Energy Fuels 2:2507–2515. https://doi.org/10.1039/C8SE00319J
19. Hong E, Kim D, Kim JH (2014) Heterostructured metal sulfide (ZnS–CuS–CdS) photocatalyst for high electron utilization in hydrogen production from solar water splitting. J Ind Eng Chem 20:3869–3874. https://doi.org/10.1016/j.jiec.2013.12.092
20. Priyadharsana A, Shanavasa S, Vasanthakumar V et al (2018) Synthesis and investigation on synergetic effect of rGO-ZnO decorated MoS_2 microflowers with enhanced photocatalytic and

antibacterial activity. Colloids Surf A Physicochem Eng Asp 559: 43–53. https://doi.org/10.1016/j.colsurfa.2018.09.034
21. Reddy DA, Choi J, Lee S et al (2015) Green synthesis of AgI nanoparticle-functionalized reduced graphene oxide aerogels with enhanced catalytic performance and facile recycling. RSC Adv 5: 67394–67404. https://doi.org/10.1039/c5ra07267k
22. Choi J, Reddy DA, Kim TK (2015) Enhanced photocatalytic activity and anti-photocorrosion of AgI nanostructures by coupling with graphene-analogue boron nitride nanosheets. Ceram Int 41:13793–13803. https://doi.org/10.1016/j.ceramint.2015.08.062
23. Choi J, Reddy DA, Islam MJ et al (2015) Green synthesis of the reduced graphene oxide-CuI quasi-shell-core nanocomposite: a highly efficient and stable solar-light-induced catalyst for organic dye degradation in water. Appl Surf Sci 358:159–167. https://doi.org/10.1016/j.apsusc.2015.07.170
24. Choi J, Reddy DA, Islam MJ et al (2016) Self-assembly of CeO_2 nanostructures/reduced graphene oxide composite aerogels for efficient photocatalytic degradation of organic pollutants in water. J Alloys Compd 688:527–536. https://doi.org/10.1016/j.jallcom.2016.07.236
25. Reddy DA, Lee S, Choi J et al (2015) Green synthesis of AgI-reduced graphene oxide nanocomposites: toward enhanced visible-light photocatalytic activity for organic dye removal. Appl Surf Sci 341:175–184. https://doi.org/10.1016/j.apsusc.2015.03.019
26. Lakhera SK, Hafeez HY, Venkataramana R et al (2019) Design of a highly efficient ternary AgI/rGO/$BiVO_4$ nanocomposite and its direct solar light induced photocatalytic activity. Appl Surf Sci 487: 1289–1300. https://doi.org/10.1016/j.apsusc.2019.05.201
27. Gunjakar JL, Kim IY, Lee JM et al (2013) Self-assembly of layered double hydroxide 2D nanoplates with graphene nanosheets: an effective way to improve the photocatalytic activity of 2D nanostructured materials for visible light-induced O_2 generation. Energy Environ Sci 6:1008. https://doi.org/10.1039/c3ee23989f
28. Yang J, Duan X, Guo W et al (2014) Electrochemical performances investigation of NiS/rGO composite as electrode material for supercapacitors. Nano Energy 5:74–81. https://doi.org/10.1016/j.nanoen.2014.02.006
29. Hafeez HY, Lakhera SK, Narayanan N, Harish S, Hayakawa Y, Lee BK, Neppolian B (2019) Environmentally sustainable synthesis of a $CoFe_2O_4$-TiO_2/rGO ternary photocatalyst: a highly efficient and stable photocatalyst for high production of hydrogen (solar fuel). ACS Omega 4:880–891. https://doi.org/10.1021/acsomega.8b03221
30. Nguyen DCT, Cho KY, Oh W-C (2017) Synthesis of mesoporous SiO_2/Cu_2O–graphene nanocomposites and their highly efficient photocatalytic performance for dye pollutants. RSC Adv 7: 29284–29294. https://doi.org/10.1039/C7RA03526H
31. An X, Yu JC (2011) Graphene-based photocatalytic composites. RSC Adv 1:1426. https://doi.org/10.1039/c1ra00382h
32. Acharya S, Martha S, Sahoo PC, Parida K (2015) Glimpses of the modification of perovskite with graphene-analogous materials in photocatalytic applications. Inorg Chem Front 2:807–823. https://doi.org/10.1039/C5QI00124B
33. Singh A, Sinha ASK (2018) Active CdS/rGO photocatalyst by a high temperature gas-solid reaction for hydrogen production by splitting of water. Appl Surf Sci 430:184–197. https://doi.org/10.1016/j.apsusc.2017.02.214
34. Bagherzadeh M, Kaveh R (2018) A new SnS_2-$BiFeO_3$/reduced graphene oxide photocatalyst with superior photocatalytic capability under visible light irradiation. J Photochem Photobiol A Chem 359:11–22. https://doi.org/10.1016/j.jphotochem.2018.03.031
35. Bu Y, Li F, Zhang Y et al (2016) Immobilizing CdS nanoparticles and MoS_2/RGO on Zr-based metal–organic framework 12-tungstosilicate@UiO-67 toward enhanced photocatalytic H_2 evolution. RSC Adv 6:40560–40566. https://doi.org/10.1039/C6RA05522B
36. Qin Y, Sun Z, Zhao W et al (2017) Improved photocatalytic properties of ZnS/RGO nanocomposites prepared with GO solution in degrading methyl orange. Nano-Structures Nano-Objects 10:176–181. https://doi.org/10.1016/j.nanoso.2017.05.005
37. Dong X, Deng Z-P, Huo L-H et al (2019) Large-scale synthesis of NiS@N and S co-doped carbon mesoporous tubule as high performance anode for lithium-ion battery. J Alloys Compd 788:984–992. https://doi.org/10.1016/j.jallcom.2019.02.326
38. Wei C, Cheng C, Cheng Y et al (2015) Comparison of NiS_2 and α-NiS hollow spheres for supercapacitors, non-enzymatic glucose sensors and water treatment. Dalton Trans 44:17278–17285. https://doi.org/10.1039/C5DT02724A
39. Han C, Yang M-Q, Zhang N, Xu Y-J (2014) Enhancing the visible light photocatalytic performance of ternary CdS–(graphene–Pd) nanocomposites via a facile interfacial mediator and co-catalyst strategy. J Mater Chem A 2:19156–19166. https://doi.org/10.1039/C4TA04151H
40. Shanavas S, Priyadharsan A, Gkanas EI et al (2019) High efficient catalytic degradation of tetracycline and ibuprofen using visible light driven novel Cu/$Bi_2Ti_2O_7$/rGO nanocomposite: kinetics, intermediates and mechanism. J Ind Eng Chem 72:512–528. https://doi.org/10.1016/j.jiec.2019.01.008
41. Lu Z, Song W, Ouyang C et al (2017) Enhanced visible-light photocatalytic performance of highly-dispersed Pt/g-C_3N_4 nanocomposites by one-step solvothermal treatment. RSC Adv 7:33552–33557. https://doi.org/10.1039/c7ra04931e
42. Chowdhury P, Gomaa H, Ray AK (2013) Dye-sensitized photocatalyst: a breakthrough in green energy and environmental detoxification. pp 231–266
43. Faraji M, Yousefi M, Yousefzadeh S et al (2019) Two-dimensional materials in semiconductor photoelectrocatalytic systems for water splitting. Energy Environ Sci 12:59–95. https://doi.org/10.1039/C8EE00886H